Causes of simulated long-term changes in phytoplankton biomass in the Baltic Proper: A wavelet analysis

Jenny Hieronymus[1], Kari Eilola[1], Magnus Hieronymus[1], H. E. Markus Meier[2,1], and Sofia Saraiva[1]

[1]Research and Development Department, Swedish Meteorological and Hydrological Institute, Norrköping, Sweden
[2]Department of Physical Oceanography and Instrumentation, Leibniz Institute for Baltic Sea Research Warnemünde, Rostock, Germany.

Correspondence to: Jenny Hieronymus (jenny.hieronymus@gmail.com)

Abstract. The co-variation of key variables with simulated phytoplankton biomass in the Baltic proper has been examined using wavelet analysis and results of a long-term simulation for 1850-2008 with a high-resolution, coupled physical-biogeochemical circulation model for the Baltic Sea. By focusing on inter-annual variations it is possible to track effects acting on decadal time scales such as temperature increase due to climate change as well as changes in nutrient input. The results indicate the largest inter-annual coherence of phytoplankton biomass with the limiting nutrient.However, after 1950 the coherence is reduced due to high mixed layer nutrient concentrations diminishing the effect of smaller long-term variations. Furthermore, the inter-annual coherence of mixed layer nitrate with riverine input of nitrate is much larger than the coherence between mixed layer phosphate and phosphate loads. This indicates a greater relative importance of mixing of phosphate from deeper layers. In addition, shifts in nutrient patterns give rise to changes in phytoplankton nutrient limitation. The modelled pattern shifts from purely phosphate limited to a seasonally varying regime. The results further indicate some effect of inter-annual temperature increase on cyanobacteria and flagellates. Changes in mixed layer depth affect mainly diatoms due to a high sinking velocity while inter-annual coherence between irradiance and phytoplankton is not found.

1 Introduction

The Baltic Sea is a semi-enclosed brackish water body separated from the North Sea and Kattegat through the Danish Straits. It stretches from about 54^o to 66^o N and the limited water exchange with the ocean in the south gives rise to a large meridional salinity gradient. The circulation is estuarine with a salty deep-water inflow from the ocean and a fresher surface outflow. The Baltic Sea comprises a number of sub-basins connected by sills further restricting the circulation.

The limited water exchange and the long residence time of water have consequences for the biology and the biogeochemistry. The Baltic Sea is naturally prone to eutrophication and organic matter degradation keeps the deep water oxygen concentrations generally low in between deep water renewal events. In turn, this leads to complex nutrient cycling with different processes acting in oxygenized vs low oxygen environments.

The Baltic Sea has experienced extensive anthropogenic pressure over the last century. After 1950, intensive use of agricultural fertilizer greatly enhanced the nutrient loads. This led to an expansion of hypoxic bottoms (Carstensen et al., 2014), in turn affecting the cycling of nutrients through the system. Anoxic sediments have lower phosphorus retention capacity resulting in

increased deep water phosphate concentrations. Thereby, the flux of phosphate to the surface intensifies even though the external loads have decreased after 1980 in response to improved sewage treatment. Furthermore, as the anoxic area increases, the area of interface between oxic and anoxic zones where denitrification occurs also increases. This results in a loss of nitrogen. Vahtera et al. (2007) described these processes as generating a "vicious circle" where decreased DIN concentrations together with increased phosphate enhance the relative importance of nitrogen fixation by cyanobacteria.

The importance of this coupling between oxygen and nutrients have been further examined in models. Gustafsson et al. (2012) confirmed, using the model BALTSEM, that internal nutrient recycling has increased due to reduced phosphate retention capacity, implicating a self sustained eutrophication where enhanced internal loads outweigh external load reductions.

Satellite monitoring has made it possible to observe changes in several physical and ecological surface variables during the past three decades. Significant changes in seasonality have been observed, such as earlier start of phytoplankton growth season and timing of chlorophyll maxima (Kahru et al., 2016).

Although the satellite record is already substantial and growing, interannual shifts and variations over the past century can not be investigated in this way. Furthermore, the satellite record is restricted to a few surface variables. Shifts in nutrient composition and deep water variables remain difficult to evaluate using observations. Even though the Baltic Sea has a dense observational record from ships, stations and satellites, the longest nutrient records comprise station data from the early 70s (HELCOM, 2012). For multidecadal periods of gap free data the use of a model is required.

In this paper we construct a thorough analysis of the co-variation of phytoplankton biomass with key variables that have been affected by anthropogenic change over the 20th century. Using the biogeochemical model SCOBI (Eilola et al., 2009; Almroth-Rosell et al., 2011) coupled to the 3d circulation model RCO we scrutinize the effect of nutrient loads, nutrient concentration, temperature, irradiance and mixed layer depth on the modelled phytoplankton community.

The gap-free dataset provided by the model lets us decompose the variables in time-frequency space using the wavelet transform. Two variables may than be compared using wavelet coherence (eg. Torrence and Compo, 1998; Grinsted et al., 2004).

We have chosen to use a model run spanning 1850-2009. Thereby, we capture conditions relatively unaffected by anthropogenic forcing as well as current conditions of eutrophication and climate change. Furthermore, we limit our investigation to the Baltic Proper so as to capture relatively homogenous conditions with regards to the biology.

Schimanke and Meier (2016) analyzed multidecadal variations in Baltic Sea salinity and the coherence with different physical drivers. They used the wavelet transform to identify periodicities and wavelet coherency to analyse the driving mechanisms.

2 Methods

2.1 Study area

The Baltic Sea contains several different sub-basins with different characteristics in salinity and nutrient loads. We have here chosen to focus on the Baltic Proper. To obtain homogenous conditions we focus on the open ocean away from coasts. Areas where the depth is less than 20m are therefore removed. The study area is displayed in Fig. 1.

We have chosen to use a basin averaged approach. All variables have thus been horizontally averaged over the study area. This way we remove local variability and hope to gain a better understanding of the system.

2.2 Model

We have used a run with the model RCO-SCOBI spanning 1850-2009. RCO (Rossby Centre Ocean model) is a three-dimensional regional ocean circulation model(Meier et al., 2003). It is a z-coordinate model with a free surface and an open boundary in the northern Kattegat. The version used here has a horizontal resolution of 2nm with 83 depth levels at 3m intervals.

The biogeochemical interactions are solved by the Swedish Coastal and Ocean Biogeochemical model (SCOBI) (Eilola et al., 2009; Almroth-Rosell et al., 2011). The model solves for three different water column and benthic nutrients (phosphate, nitrate and ammonia) as well as plankton functional types representing diatoms, flagellates and others (will be referred to as flagellates from here on) and cyanobacteria. Furthermore, the model contains nitrogen and phosphorus in one active homogenous benthic layer.

The model equations can be found in Eilola et al. (2009). Since we are exploring the effect of different variables on the growth of phytoplankton we will, for clarity, repeat some of them here.

The phytoplankton biomass is described in terms of chlorophyll and with a constant C:Chl ratio. The model thus does not take into account seasonal changes in C:Chl as was found by Jakobsen and Markager (2016).

The net growth of phytoplankton is described by the following expression,

$$\mathrm{GROWTH_{PHY}} = \mathrm{ANOX} \cdot \mathrm{LTLIM} \cdot \mathrm{NUTLIM_{PHY}} \cdot \mathrm{GMAX_{PHY}} \cdot \mathrm{PHY}, \quad (1)$$

where subscript PHY indicates the plankton funktional type (diatoms, flagellates or cyanobacteria). ANOX is a logarithmic expression that approaches zero as the oxygen concentration becomes small.

LTLIM expresses the phytoplankton light limitation and NUTLIM describes the nutrient limitation. Nutrient limitation follows Michaelis-Menten kinetics where constant Redfield ratios are assumed in nutrient uptake. NUTLIM is further described in Sects. 2.2.1 and 2.2.2. GMAX is temperature dependent and describes the maximum phytoplankton growth rate.

The difference between diatoms and flagellates are present in halfsaturation constants, maximum growth rate, temperature dependence and sinking rate. Flagellates are more sensitive to a change in temperature than diatoms. Furthermore, the sinking rate of diatoms is five times larger than that for flagellates.

The difference between cyanobacteria and the other phytoplankton species is more pronounced. Cyanobacteria can grow either according to Eq. (1) or using nitrogen fixation. The rate of nitrogen fixation as a function of the phosphate concentration and temperature. Both NFIX and GROWTH of cyanobacteria is zero if the salinity is above 10. Furthermore, cyanobacteria is the most temperature sensitive of the phytoplankton groups and no sinking velocity is assumed.

Other processes important for our results involves chemical reactions occurring in the water column or in the sediment. Denitrification occurs in both the water column and the benthic layer and constitutes a sink for nitrate in case of anoxia. Nitrification transforms ammonium into nitrate as long as oxygen is present. Phosphorus is adsorbed to the sediment and the

benthic release capacity of phosphate is a function of the oxygen concentration where more oxygen implies less release. The phosphorus release capacity is also dependent on salinity where higher salinity means less phosphate is retained in the benthic layer.

2.2.1 Nutrient limitation

Estimating nutrient limitation in nature is difficult. Usually this is done, either by comparing nutrient ratios to Redfield in eg. the surface water or external supply or by some nutrient enrichment experiment (Granéli et al., 1990).

The idea of nutrient limitation as often used is based on that the primary production is directly limited by the nutrient concentration in the ambient water and that the internal nutrient ratios in the phytoplankton are constant, i.e. in accordance with a Redfield-Monod model (Redfield, 1958). However, cell-quota type models (Droop, 1973) are being increasingly implemented and the use of constant internal nutrient ratios are becoming more and more questioned (Flynn, 2010).

Furthermore, N vs P limitation is a long standing debate. Tyrrell (1999) uses a box-modelling approach to show that in steady state, nitrogen becomes slightly deficient while it is the external input and removal of phosphate that ultimately controls the production.

Here, nutrient limitation is traditionally expressed assuming constand Redfield ratios and phytoplankton growth is limited by either nitrogen or phosphate. The degree of nutrient limitation is described by:

$$\mathrm{NUTLIM_{PHY}} = \min(\mathrm{NLIM_{PHY}}, \mathrm{PLIM_{PHY}}) \tag{2}$$

where $\mathrm{NLIM_{PHY}}$ and $\mathrm{PLIM_{PHY}}$ are the nitrogen and phosphate limitation respectively. In addition, $\mathrm{NLIM_{PHY}}$ contains the sum of the nitrate and ammonium limitation, i.e.

$$\mathrm{NLIM_{PHY}} = \mathrm{NO_3LIM_{PHY}} + \mathrm{NH_4LIM_{PHY}}, \tag{3}$$

where

$$\mathrm{NO_3LIM} = \frac{\mathrm{NO3}}{\mathrm{KNO3_{PHY}} + \mathrm{NO3}} \cdot \exp(-\phi_{\mathrm{PHY}} \cdot \mathrm{NH_4}), \tag{4}$$

$$\mathrm{NH_4LIM} = \frac{\mathrm{NH4}}{\mathrm{KNH4_{PHY}} + \mathrm{NH4}}, \tag{5}$$

where NO3 and NH4 are the concentrations of nitrate and ammonium and $\mathrm{KNO3_{PHY}}$ and $\mathrm{KNH4_{PHY}}$ are the halfsaturation constants for nitrate and ammonium respectively. The exponent in (4) accounts for inhibition of nitrate uptake (eg. Dortch (1990); Parker (1993)).

$\mathrm{PLIM_{PHY}}$ is modelled as,

$$\mathrm{PO_4LIM} = \frac{\mathrm{PO4}}{\mathrm{KPO4_{PHY}} + \mathrm{PO4}}. \tag{6}$$

Nutrient limitation is thus described by a number between 0 and 1 where 1 is no limitation. Note that NLIM in Eq. (3) may obtain values larger than 1. However, as NUTLIM is calculated as the minimum of NLIM and PLIM, NLIM larger than one will always mean P limitation.

The constants $\mathrm{KNO3_{PHY}}$, $\mathrm{KNH4_{PHY}}$ and $\mathrm{KPO4_{PHY}}$ are the half saturation constants and differs between the different phytoplankton groups. The constant ϕ_{PHY} in Eq. (4) determines the strength of ammonium inhibition of nitrate uptake.

2.2.2 Effect of physical parameters

Changes in cloud-cover affect the incoming solar radiation and thereby the phytoplankton growth. The effect of light shows up in the LTLIM term of Eq. (1).

The mixed layer depth has been defined as the depth where a density difference of 0.125 kg $\mathrm{m^{-3}}$ from the surface is reached in accordance with what was previously done by e.g. Eilola et al. (2013). The density was calculated from modelled temperature and salinity using the algorithms from Jackett et al. (2006).

2.3 Forcing

The study use reconstructed (1850-2008) atmospheric, hydrological and nutrient load forcing and daily sea levels at the lateral boundary as described by Gustafsson et al. (2012) and Meier et al. (2012). Monthly mean river flows were merged from reconstructions done by Hansson et al. (2011) and by Meier and Kauker (2003) and hydrological model data by Graham (1999), respectively. For further details about the physical model setup used in the present study the reader is referred to Meier et al. (2016) and references therein.

The nutrient loads from rivers and point sources were (1970-2006) compiled from the Baltic Environmental and HELCOM databases (Savchuk et al., 2012). Estimates of pre-industrial loads for 1900 were based upon Savchuk et al. (2008). The nutrient loads were linearly interpolated between selected reference years in the period between 1900 and 1970. Similarly, atmospheric loads were estimated (Ruoho-Airola et al., 2012). Nutrient loads contain both organic and inorganic phosphorus and nitrogen, respectively. For riverine organic phosphorus and nitrogen loads bioavailable fractions of 100 and 30% are assumed, respectively.

Figure 2 shows the loads of Dissolved Inorganic Phosphorus (DIP, top) and Dissolved Inorganic Nitrogen (DIN, bottom) to the Baltic Proper as defined in Fig. 1. The loads are shown together with the corresponding simulated mixed layer concentration. The loads are calculated from the runoff and annual mean nutrient concentrations (Eilola et al., 2011). Thus the seasonal cycle in river loads is determined by the runoff. After a spin-up simulation for 1850-1902 utilizing the reconstructed forcing as described above, the calculated physical and biogeochemical variables at the end of the spin-up simulation were used as initial condition for 1850.

The open boundary conditions in the northern Kattegat were based on climatological (1980-2000) seasonal mean nutrient concentrations (Eilola et al., 2009). Similar to Gustafsson et al. (2012) a linear decrease of nutrient concentrations back in time was added assuming that climatological concentrations in 1900 amounted to 85% of present day concentrations (Savchuk et al., 2008). The bioavailable fraction of organic phosphorus at the boundary was assumed to be 100% in accordance with

the organic phosphorus supply from land runoff. Organic nitrogen was implicitly added because of the Redfield ratio of model detritus (Eilola et al., 2009).

2.4 The wavelet transform and wavelet coherence

Several references explain the wavelet transform and its application in depth (e.g. Lau and Weng (1995), Torrence and Compo (1998), Carey et al. (2016), Grinsted et al. (2004)) and we will here provide a brief introduction.

The continuous wavelet transform provides a method to decompose a signal into time-frequency space. In that it is similar to the windowed Fourier transform where the signal is decomposed within a fixed time-frequency window which is then slided along the time-series. However, the fixed width of the window leads to an underestimation of low frequencies. In comparison, the wavelet transform utilizes wavelets with a variable time-frequency window. Wavelets can have many different shapes and the choice is not arbitrary. We have chosen the commonly used Morlet wavelet providing good time and frequency localization (Grinsted et al., 2004).

In time-series with clear periodic patterns that is affected by environmental variables such as population dynamics and ecology the benefits with this approach are significant (Cazelles et al., 2008). In recent years, several references have highlighted the usefulness of wavelet analyses in plankton research (Winder and Cloern, 2010; Carey et al., 2016). The focus have been the increased availability of long observational data sets making it possible to use the wavelet transform for investigation of changes in seasonality. Carey et al. (2016) discussed how the wavelet transform can be used to track interannual changes in phytoplankton biomass and applied it to a 16-year time series of phytoplankton in Lake Mendota, USA. In doing this they were able to identify periods when the annual periodicity was less pronounced. They discuss the benefit of this technique in scrutinizing changes to the seasonal succession due to changes in external drivers. Winder and Cloern (2010) applied the technique to time-series of chlorophyll-a from marine and freshwater localities and discussed the annual and seasonal periodicities.

Wavelet coherence further expands the usefulness of the wavelet approach by allowing for calculating the time resolved coherence between two time-series (Grinsted et al., 2004; Cazelles et al., 2008). In this way, it is possible to identify transient periods of correlation over different periodicities. The result is given as coherency as a function of time and period as well as a phase lag between the two time-series.

The problem with the wavelet transform is that it requires a dataset without gaps. The time-series also needs to be sufficiently long compared to the investigated periods. This makes it difficult to use the method to scrutinize the coherence of processes acting on longer time-scales, such as climate change, since long enough observational datasets are scarce. Hence, for our purpose only a model based approach is feasible.

Schimanke and Meier (2016) used wavelet coherency on a multi-centennial model run to evaluate the correlation of different forcing variables with the Baltic Sea salinity. We will here scrutinize the coherence between modelled phytoplankton biomass and a few key modelled and forcing variables.

For all wavelet calculations we use the Matlab wavelet package of described in Grinsted et al. (2004), which is freely available at http://www.glaciology.net/wavelet-coherence.

3 Results and discussion

The results shown are monthly means averaged over the basin. The different variables have also been vertically averaged over the mixed layer and/or from the mixed layer down to a depth of 150m.

We will begin in Sect. 3.1 by presenting the model results of phytoplanton biomass. In Section 3.2 we will consider the composition of nutrients and the coherence with the phytoplankton biomass. Coherence between riverine loads and mixed layer nutrients will be discussed in Sect. 3.3. Section 3.4 examines the coherence of phytoplankton with temperature and irradiance. Finally, the coherence between mixed layer depth and phytoplankton biomass is considered in Sect. 3.5.

3.1 Phytoplankton biomass

Fig. 3 shows the time-series of phytoplankton biomass (a) together with the corresponding wavelet spectrum (b).

The wavelet power (variance) of the decomposed signal (in color) is displayed as a function of time (x-axis) and period (y-axis). The black curves in Fig. 3(b) show the 95% confidence level relative to red noise.

Averaging over time generates the global power spectrum displayed in Fig. 3 (c). The wavelet spectrum clearly reveals two main periodicities - the annual and the semi-annual representing the spring and autumn blooms. It is also clearly visable that the power on both periodicities increases markedly after 1950.

Kahru et al. (2016) found a shift in chlorophyll maxima from the diatom dominated spring bloom to the cyanobacteria summer bloom. Fig. 4 shows that a similar pattern emerges from our model run with five years of cyanobacterial chlorophyll maxima occurring after 1998.

3.2 Nutrients and nutrient limitation

The extent of anoxic bottoms in the Baltic Sea has increased markedly over the past century. Carstensen et al. (2014) found a 10-fold increase in the hypoxic area since the beginning of the 20th century. They explained this to be primarily due to increased nutrient loads causing increased primary production and resulting in an enhanced deep water respiration.

Changing nutrient patterns in the Baltic Sea due to spreading hypoxia have been discussed by e.g. Conley et al. (2002); Savchuk (2010); Vahtera et al. (2007). Anoxia causes sedimentary phosphate release. A clear relationship between hypoxia and total basin averaged phosphate was first shown by Conley et al. (2002) (and later expanded by Savchuk (2010)) on observational data from the Baltic Proper.

The effect of hypoxia on DIN is less straight forward. Expanding hypoxia increases the boundary area between anoxic and oxic water where denitrification occurs resulting in a further loss of nitrate. Furthermore, hypoxia induced reduction in nitrification results in a loss of nitrate. Vahtera et al. (2007) found a negative relationship between basin averaged DIN and hypoxic area in observations from the Baltic sea.

We illustrate the changing nutrient patterns for our model run in Fig. 5. In conjunction with the increased anoxic volume we find a clear increase in ammonium and a decrease in nitrate. This is due to a decrease in nitrification and an increase

in denitrification. The phosphate concentration increases from the mid 20th century through the rest of the model run as a combined effect of the accumulated terrestrial inputs and hypoxic sedimentary release.

The effect of nutrients on the primary production is in the model controlled by the term NUTLIM, or degree of nutrient limitation, in Eq. (1). NUTLIM can be viewed as a measure of the nutrient composition that linearly affects the phytoplankton growth in the model. We will examine this term in and below the mixed layer. Even though there is no primary production in the deep water and thus the nutrient limitation term has no effect here, a shift in the composition of nutrients in the deep water will affect also the mixed layer. NUTLIM for diatoms and flagellates has been calculated offline from the monthly means according to Eq. (2).

The evolution of NUTLIM in the surface layer and the deep water for diatoms and flagellates is shown in Fig. 6. There is a clear increase over the 20th century and a shift towards less limited conditions (NUTLIM approaching 1).

Nitrogen has been shown to most often be limiting in the Baltic Proper, while phosphate is limiting in the northern basins (Granéli et al., 1990; Tamminen and Andersen, 2007). Schernewski and Neumann (2004) showed through a reconstruction of the Baltic Sea trophic state in the early 1900 that N/P ratios in the Baltic Proper have decreased but that much of the domain still indicated N limitation.

Using the models definition of nutrient limitation, our model results, shown in Fig. 7, display phosphate limitation for both diatoms and flagellates for the earlier part of the run. After 1980, seasonality appears in the mixed layer. Phosphate is still limiting during winter while nitrogen becomes limiting after the spring bloom. Calculating N/P ratios as a more conventional measure of nutrient limitation, our model results diplay instead a shifting pattern until 1976 whereafter persistant N limitation develops (not shown).

The changing nutrient patterns affects the phytoplankton growth. We analyse the wavelet coherencies of phytoplankton biomass with mixed layer phosphate and DIN in Figs. 8 and 9.

Coherency is shown in color as a function of year (x-axis) and period (y-axis). More yellow indicates stronger coherence. The arrows reveal the phase-lag between the two time-series. The line plots on the right show the time averaged coherence. As the strongest nutrient limited group, diatoms show persistant inter-annual coherence with phosphate during the first, consistently phosphate limited part of the run (see Fig. 7). During the later part of the run the nutrient and phytoplankton concentrations are high enough that smaller inter-annual variations have little effect.

Since nitrogen limitation in the model only occurs after 1980 and after the spring bloom and thus only affects the much smaller diatom and flagellate autumn blooms no coherence between phytoplankton and nitrogen is visable in Fig. 9.

To scrutinze the shift in deep water nutrient composition and the coherence with phytoplankton, we calculate the wavelet coherence between below mixed layer NUTLIM and the diatom and flagellate biomass. The result is shown in Fig. 10. The phase arrows here display some interesting features. After 1980 the phase arrows within the annual coherence period change to the opposite direction. For diatoms, the phase shifts from NUTLIM preceding diatoms by three months to diatoms preceding nutlim by the same amount. Flagellates display a similar shift.

To investigate this, we have plotted the month of maximum NUTLIM in Fig. 11. The figures show a clear shift occuring after 1980. Below the mixed layer, NUTLIM changes its maxima from December and January to July, August and September

while a slight shift from February to March is apparent for diatoms. Mixed layer NUTLIM for flagellates displays no clear shift.

3.3 Nutrient loads

The wavelet coherence between mixed layer nutrients and riverine input is shown in Fig. 12. We have used riverine DIN and DIP loads in the results presented below. The use of instead total bioavailable nutrient loads does not change the results.

The phosphate loads show little coherence on periodicities longer than one year but DIN displays strong inter-annual coherence. The phase-arrows indicate a phase-lag of about minus 45° on all inter-annual periodicities. For an 8 year period this means that riverine input precedes DIN by about 1 yr.

To further investigate the lack of inter-annual coherence between riverine phosphate loads and mixed layer phosphate, the wavelet coherence between mixed layer salinity and nutrients are examined and displayed in Fig. 13. Mixed layer salinity is affected by freshwater input from land, precipitation, evaporation and mixing with deeper layers. The coherence spectrum reveals higher coherence between mixed layer salinity and phosphate (top) on interannual periodicities than between salinity and DIN (bottom). The coherence existing between salinity and DIN on periodicities longer than one year is antiphase i.e. low salinity here coheres with high DIN concentrations. In contrast, the in-phase coherence between salinity and phosphate suggests that the reason for the coherence might be a greater importance of phosphorus release from the sediments that eventually reaches the mixed layer through mixing with deeper layers.

Riverine nutrient loads show little inter-annual coherence with phytoplankton biomass (not shown) other than on a 16 yr period which probably reflects the overall pattern of simultaneous increase in riverine loads and phytoplankton biomass over the second half of the 20th century.

3.4 Temperature and irradiance

The mixed layer temperature has increased over the 20th century. Figure 14 shows the 2-yr moving average of mixed layer temperature. To scrutinize the effect of temperature on the concentration of phytoplankton, the wavelet coherence between temperature and phytoplankton have been plotted in Fig. 15. The results suggest that the temperature increase after 1990 might have had an effect on cyanobacteria and flagellates. It is also noticable that the temperature increase observed between 1900 and 1940 probably had an effect on cyanobacteria. This is also in agreement with the model formulation where cyanobacteria are the most sensitive to temperature followed by flagellates.

Light impacts primary production through the term LTLIM in Eq. (1). However, irradiance display very little variation on any other periodicity than the annual as can be observed in a wavelet power spectrum (not shown). Therefore there exists almost no coherence between phytoplankton and irradiance apart from the annual and semiannual.

3.5 Mixed layer depth

The lower panel of Fig. 14 shows the two year moving average of mixed layer depth averaged over the basin. We calculate the coherence between mixed layer depth and diatoms, flagellates and cyanobacteria in Fig. 16.

Apart from the annual cycle there is a strong coherence between mixed layer depth and diatoms, and to some extent flagellates, on shorter periodicities as well. That is, the concentration of diatoms residing in the mixed layer seems to covary quite well on periodicities equal to or shorter than one year. The model value for diatom sinking rate is five times higher than that for flagellates while cyanobacteria is assumed to have no sinking rate. In a shallow mixed layer the diatom concentration decreases faster than in a deep mixed layer because of the large sinking rate. In the wavelet coherence spectrum we thus see in-phase short term coherence.

4 Summary and conclusions

With a focus on inter-annual variations, the coherence of the mixed layer phytoplankton biomass with key variables affecting the primary production has been examined for the Baltic Proper.

We found that the pattern of nutrient limitation in and below the mixed layer have changed in the model since 1980. Below the mixed layer, the limitation pattern changes from phosphate to nitrogen for diatoms and to seasonally shifting between phosphate and nitrogen. Within the mixed layer, the pattern changes from pure phosphate limitation to seasonally shifting for both diatoms and flagellates. This is due to decreased deep water oxygen concentrations and a rapid expansion of anoxia after 1970. The phosphate concentrations increase due to enhanced sedimentary release, denitrification results in loss of nitrate and reduced nitrification decreases the transformation of ammonium to nitrate. The combined effect results in nitrogen limitation after the spring bloom which benefits cyanobacteria.

The mixed layer concentrations of nutrients affect the primary production in the model through the nutrient limitation term, NUTLIM. The phytoplankton group most strongly limited by nutrients in the model is diatoms. The connection between primary production and the nutrient limitation term is visable as a strong inter-annual coherence between diatoms and phosphate as well as NUTLIM before 1940. After 1940 NUTLIM and the concentrations of the individual phytoplankton species have gained such high values that smaller inter-annual variations have little effect on the production. Similarily, the less nutrient sensitive group flagellates shows much smaller inter-annual coherence with phosphate even before 1940. NUTLIM for this group is already high enough so that small long-term variations do not reflect strongly in the results.

Very little inter-annual coherence is visable also between phytoplankton and nitrogen. The spring bloom is phosphate limited throughout the run except for a few years after 1990 where diatoms display nitrogen limitation. The much weaker diatom and flagellate autumn bloom displays no inter-annual coherence with DIN most likely due to the high NUTLIM levels.

The shift in nutrient limitation patterns is also visable in a slight forward shift in the month of maximum mixed layer NUTLIM for diatoms after 1980, although a similar shift cannot be seen for flagellates. Below the mixed layer, maximum NUTLIM shifts significantly towards late summer for both diatoms and flagellates. Furthermore, the annual maximum of total chlorophyll concentration (Diatoms + Flagellates + Cyanobacteria) displayed a few years at the end of the run where the

maximum corresponded to the autumn bloom due to the large increase in cyanobacteria. This is in agreement with Kahru et al. (2016) who found from satellite data that the annual chlorophyll maximum has shifted from the spring bloom maximum in May to the cyanobacteria bloom in July.

Riverine input of nutrients is an extremely important variable in the Baltic Sea and the large increase during the 20th century has initiated spreading of anoxic bottoms (Carstensen et al., 2014). We found quite strong coherence between riverine input of DIN and mixed layer DIN but not a similar relationship between riverine phosphate input and the corresponding mixed layer concentration. As mixed layer salinity displayed in-phase inter-annual coherence with phosphate and only weak anti-phase coherence with DIN we hypothesise that this is due to a greater importance of the flux of phosphate from lower layers.

The mixed layer temperature in the Baltic Proper has increased during the 20th century. We found some response of this mainly from the most temperature sensitive phytoplankton group cyanobacteria during periods of large interannual temperature increases. Flagellates, being more temperature sensitive than diatoms, seems to display a coherence with the temperature increase occuring after 1980.

Variations in mixed layer depth affects mainly diatoms as these have a high sinking velocity. In-phase coherence on periodicities shorter than one year indicates that large seasonal changes in the mixed layer depth significantly affects the mixed layer concentrations while smaller interannual variations are of little consequence.

Irradiance displayed very little coherence with phytoplankton biomass.

In conclusion, through studying inter-annual wavelet coherence between simulated phytoplankton biomass and key variables we have found that phytoplankton showed strong coherence with the limiting nutrient before 1950. After that nutrients and phytoplankton exists in the water column at such high concentrations that smaller interannual variations have much less effect. Furthermore, the mixed layer concentrations of DIN show strong interannual coherence with riverine DIN input while riverine phosphate displays almost no coherence with the corresponding mixed layer concentration. Instead, in-phase coherence with mixed layer salinity indicates a stronger importance of mixing with lower layers. Temperature displays some inter-annual coherence with the more temperature sensitive flagellates.

5 Data availability

The model data on which the results in the present study are based on are stored and available from the Swedish Meteorological and Hydrological Institute. Please send your request to ocean.data@smhi.se.

Acknowledgements. This work was funded by the Swedish Research Council (VR) within the project " Reconstruction and projecting Baltic Sea climate variability 1850-2100" (Grant 2012-2117).

Funding was also provided by the Swedish Research Council for Environment, Agricultural Sciences and Spatial Planning (FORMAS) within the project "Cyanobacteria life cycles and nitrogen fixation in historical reconstructions and future climate scenarios (1850-2100) of the Baltic Sea" (grant no. 214-2013-1449). The study contributes also to the BONUS BalticAPP (Wellbeing from the Baltic Sea - applications

342 combining natural science and economics) project which has received funding from BONUS, the joint Baltic Sea research and development
343 programme.
344 This research is also part of the BIO-C3 project and has received funding from BONUS, the joint Baltic Sea research and development
345 programme (Art 185), funded jointly from the European Union's Seventh Programme for research, technological development and demon-
346 stration and from national funding institutions.

References

Almroth-Rosell, E., Eilola, K., Meier, H. E. M., and Hall, P. O. J.: Transport of fresh and resuspended particulate organic material in the Baltic Sea - a model study, Journal of Marine Systems, doi:doi:10.1016/j.jmarsys.2011.02.005, 2011.

Carey, C. C., Hanson, P. C., Lathrop, R. C., and St. Amand, A. L.: Using wavelet analyses to examine variability in phytoplankton seasonal succession and annual periodicity, Journal of Plankton Research, 38, 27–40, doi:10.1093/plankt/fbv116, http://www.plankt.oxfordjournals.org/lookup/doi/10.1093/plankt/fbv116, 2016.

Carstensen, J., Andersen, J. H., Gustafsson, B. G., and Conley, D. J.: Deoxygenation of the Baltic Sea during the last century, Proceedings of the National Academy of Sciences, 111, 5628–5633, doi:10.1073/pnas.1323156111, http://www.pnas.org/cgi/doi/10.1073/pnas.1323156111, 2014.

Cazelles, B., Chavez, M., Berteaux, D., Ménard, F., Vik, J. O., Jenouvrier, S., and Stenseth, N. C.: Wavelet analysis of ecological time series, Oecologia, 156, 287–304, doi:10.1007/s00442-008-0993-2, 2008.

Conley, D. J., Humborg, C., Rahm, L., Savchuk, O. P., and Wulff, F.: Hypoxia in the Baltic Sea and Basin-Scale Changes in Phosphorus Biogeochemistry, Environ. Sci. Technol., 36, 5315–5320, doi:10.1021/es025763w, 2002.

Dortch, Q.: The interaction between ammonium and nitrate uptake in phytoplankton, Marine Ecology Progress Series, 61, 183–201, doi:10.3354/meps061183, 1990.

Droop, M.: Some thoughts on nutrient limitation in algae, Journal of Phycology, 9, 264–272, doi:10.1111/j.1529-8817.1973.tb04092.x, 1973.

Eilola, K., Meier, H. E. M., and Almroth, E.: On the dynamics of oxygen, phosphorus and cyanobacteria in the Baltic Sea; A model study, Journal of Marine Systems, 75, 163–184, doi:10.1016/j.jmarsys.2008.08.009, http://dx.doi.org/10.1016/j.jmarsys.2008.08.009, 2009.

Eilola, K., Gustafsson, B. G., Kuznetsov, I., Meier, H. E. M., Neumann, T., and Savchuk, O. P.: Evaluation of biogeochemical cycles in an ensemble of three state-of-the-art numerical models of the Baltic Sea, Journal of Marine Systems, 88, 267–284, doi:10.1016/j.jmarsys.2011.05.004, http://dx.doi.org/10.1016/j.jmarsys.2011.05.004, 2011.

Eilola, K., Mårtensson, S., and Meier, H. E. M.: Modeling the impact of reduced sea ice cover in future climate on the Baltic Sea biogeochemistry, Geophysical Research Letters, 40, 149–154, doi:10.1029/2012GL054375, 2013.

Flynn, K. J.: Ecological modelling in a sea of variable stoichiometry: Dysfunctionality and the legacy of Redfield and Monod, Progress in Oceanography, 84, 52–65, doi:10.1016/j.pocean.2009.09.006, http://dx.doi.org/10.1016/j.pocean.2009.09.006, 2010.

Graham, L. P.: Modeling runoff to the Baltic Sea, Ambio, 28, 328–334, 1999.

Granéli, E., Wallström, K., Larsson, U., Granéli, W., and Elmgren, R.: Nutrient limitation of primary production in the Baltic Sea Area, Ambio, 19, 1990.

Grinsted, a., Moore, J. C., and Jevrejeva, S.: Application of the cross wavelet transform and wavelet coherence to geophysical time series, Nonlinear Processes in Geophysics, 11, 561–566, doi:10.5194/npg-11-561-2004, http://www.nonlin-processes-geophys.net/11/561/2004/, 2004.

Gustafsson, B. G., Schenk, F., Blenckner, T., Eilola, K., Meier, H. E. M., Müller-Karulis, B., Neumann, T., Ruoho-Airola, T., Savchuk, O. P., and Zorita, E.: Reconstructing the development of baltic sea eutrophication 1850-2006, Ambio, 41, 534–548, doi:10.1007/s13280-012-0318-x, 2012.

Hansson, D., Eriksson, C., Omstedt, A., and Chen, D.: Reconstruction of river runoff to the Baltic Sea, AD 1500-1995, International Journal of Climatology, 31, 696–703, doi:10.1002/joc.2097, 2011.

HELCOM: Approaches and methods for eutrophication target setting in the Baltic Sea region., Balt. Sea Env. Proc. No. 1, 2012., 2012.

Jackett, D. R., McDougall, T. J., Feistel, R., Wright, D. G., and Griffies, S. M.: Algorithms for density, potential temperature, conservative temperature, and the freezing temperature of seawater, Journal of Atmospheric and Oceanic Technology, 23, 1709–1728, doi:10.1175/JTECH1946.1, 2006.

Jakobsen, H. H. and Markager, S.: Carbon-to-chlorophyll ratio for phytoplankton in temperate coastal waters: Seasonal patterns and relationship to nutrients, Limnol. Oceanogr., 61, 1853–1868, doi:10.1002/lno.10338, 2016.

Kahru, M., Elmgren, R., and Savchuk, O. P.: Changing seasonality of the Baltic Sea, Biogeosciences, 13, 1009–1018, doi:10.5194/bg-13-1009-2016, 2016.

Lau, K. and Weng, H.: Climate signal detection using wavelet transform: How to make a time series sing, Bulletin of the American Meteorological Society, 76, 2391–2402, doi:10.1175/1520-0477(1995)076<2391:csduwt>2.0.co;2, 1995.

Meier, H. E. M. and Kauker, F.: Modeling decadal variability of the Baltic Sea : 2 . Role of freshwater inflow and large-scale atmospheric circulation for salinity, Journal of Geofphysical Research, 108, 1–16, doi:10.1029/2003JC001799, 2003.

Meier, H. E. M., Döscher, R., and Faxén, T.: A multiprocessor coupled ice- ocean model for the Baltic Sea: application to the salt inflow., Journal of geophysical research, 108, doi:10.1029/2000JC000521, 2003.

Meier, H. E. M., Andersson, H. C., Arheimer, B., Blenckner, T., Chubarenko, B., Donnelly, C., Eilola, K., Gustafsson, B. G., Hansson, A., Havenhand, J., Höglund, A., Kuznetsov, I., MacKenzie, B. R., Müller-Karulis, B., Neumann, T., Niiranen, S., Piwowarczyk, J., Raudsepp, U., Reckermann, M., Ruoho-Airola, T., Savchuk, O. P., Schenk, F., Schimanke, S., Väli, G., Weslawski, J.-M., and Zorita, E.: Comparing reconstructed past variations and future projections of the Baltic Sea ecosystem—first results from multi-model ensemble simulations, Environmental Research Letters, 7, 034 005, doi:10.1088/1748-9326/7/3/034005, 2012.

Meier, H. E. M., Höglund, A., Eilola, K., and Almroth-Rosell, E.: Impact of accelerated future global mean sea level rise on hypoxia in the Baltic Sea, Climate Dynamics, pp. 1–10, doi:10.1007/s00382-016-3333-y, 2016.

Parker, R. A.: Dynamic models for ammonium inhibition of nitrate uptake by phytoplankton, Ecological Modelling, 66, 113–120, doi:10.1016/0304-3800(93)90042-Q, 1993.

Redfield, A. C.: The biological control of chemical factors in the environment, American Scientist, 46, 205–221, doi:10.5194/bg-11-1599-2014, 1958.

Ruoho-Airola, T., Eilola, K., Savchuk, O. P., Parviainen, M., and Tarvainen, V.: Atmospheric nutrient input to the baltic sea from 1850 to 2006: A reconstruction from modeling results and historical data, Ambio, 41, 549–557, doi:10.1007/s13280-012-0319-9, 2012.

Savchuk, O. P.: Large-Scale Dynamics of Hypoxia in the Baltic Sea, in: Chemical structure of pelagic redox interfaces: Observation and modeling, Hdb Env Chem, edited by Yakushev, E. V., pp. 137–160, Springer-Verlag, Berlin Heidelberg, doi:10.1007/698_2010_53, 2010.

Savchuk, O. P., Wulff, F., Hille, S., Humborg, C., and Pollehne, F.: The Baltic Sea a century ago — a reconstruction from model simulations, verified by observations, Journal of Marine Systems, 74, 485–494, doi:10.1016/j.jmarsys.2008.03.008, http://linkinghub.elsevier.com/retrieve/pii/S0924796308000572, 2008.

Savchuk, O. P., Gustafsson, B. G., Rodríguez, M., Sokolov, A. V., and Wulff, F. V.: External nutrient loads to the Baltic Sea , 1970-2006, 2012.

Schernewski, G. and Neumann, T.: The trophic state of the Baltic Sea a century ago: a model simulation study, Journal of marine systems, 53, 109–124, doi:https://doi.org/10.1016/j.jmarsys.2004.03.007, 2004.

Schimanke, S. and Meier, H.: Decadal to centennial variability of salinity in the Baltic Sea, Journal of Climate, pp. JCLI–D–15–0443.1, doi:10.1175/JCLI-D-15-0443.1, http://journals.ametsoc.org/doi/10.1175/JCLI-D-15-0443.1, 2016.

Tamminen, T. and Andersen, T.: Seasonal phytoplankton nutrient limitation patterns as revealed by bioassays over Baltic Sea gradients of salinity and eutrophication, Marine Ecology Progress Series, 340, 121–138, doi:10.3354/meps340121, 2007.

Torrence, C. and Compo, G. P.: A practical guide to wavelet analysis, Bull. Amer. Meteor. Soc., pp. 61–78, 1998.

Tyrrell, T.: The relative influences of nitrogen and phosphorus on oceanic primary production, Nature, 400, 525–531, 1999.

Vahtera, E., Conley, D. J., Gustafsson, B. G., Kuosa, H., Pitkanen, H., Savchuk, O. P., Tamminen, T., Viitasalo, M., Wasmund, N., and Wulff, F.: Internal Ecosystem Feedbacks Enhance Nitrogen-fixing Cyanobacteria., Ambio, 36, 186–193, 2007.

Winder, M. and Cloern, J. E.: The annual cycles of phytoplankton biomass., Philosophical transactions of the Royal Society of London. Series B, Biological sciences, 365, 3215–26, doi:10.1098/rstb.2010.0125, http://rstb.royalsocietypublishing.org/content/365/1555/3215, 2010.

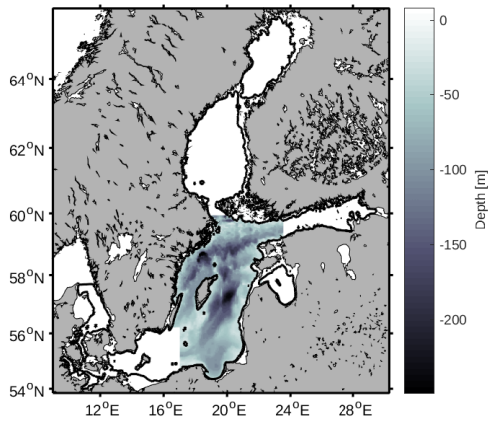

Figure 1. Study area. The grey scale represents depth in m.

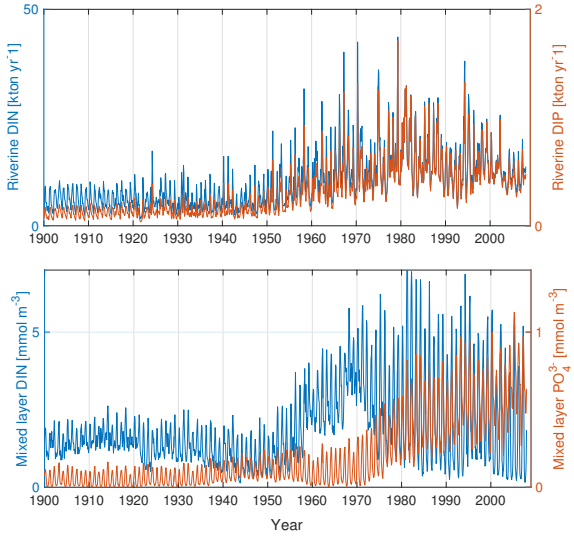

Figure 2. The top panel shows riverine DIN (blue) and phosphate (red) loads. The bottom panel shows mixed layer DIN (blue) and phosphate (red).

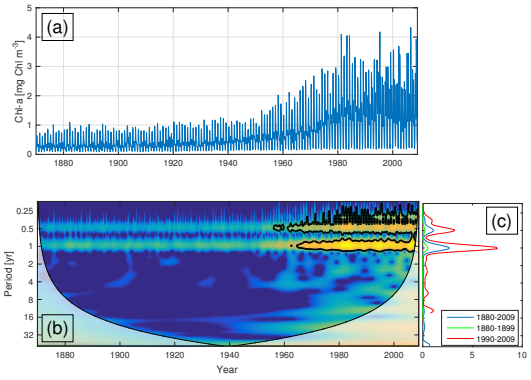

Figure 3. Time-series of phytoplankton biomass (a) together with the corresponding wavelet power spectrum (b) and global wavelet spectrum (c). More yellow means more power. The black curves in (b) represent the 95% confidence level relative to red noise. The white areas in (b) represent the cone of influence in which the results are impacted by edge-effects and are therefore not shown. The different lines in represent the global spectrum 1880-2009 (blue), 1880-1899 (green), 1990-2009 (red).

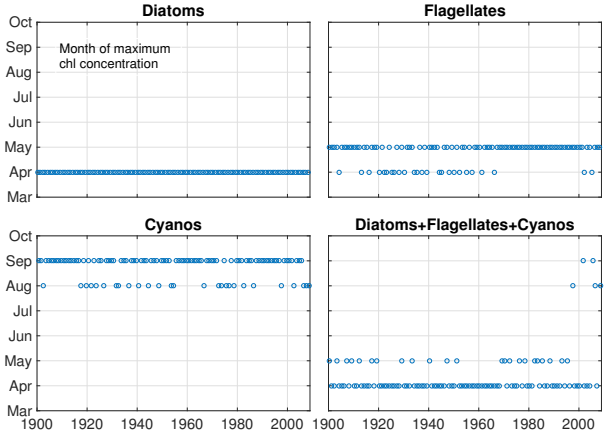

Figure 4. The month of maximum concentration of diatoms, flagellates and cyanobacteria as well as their sum.

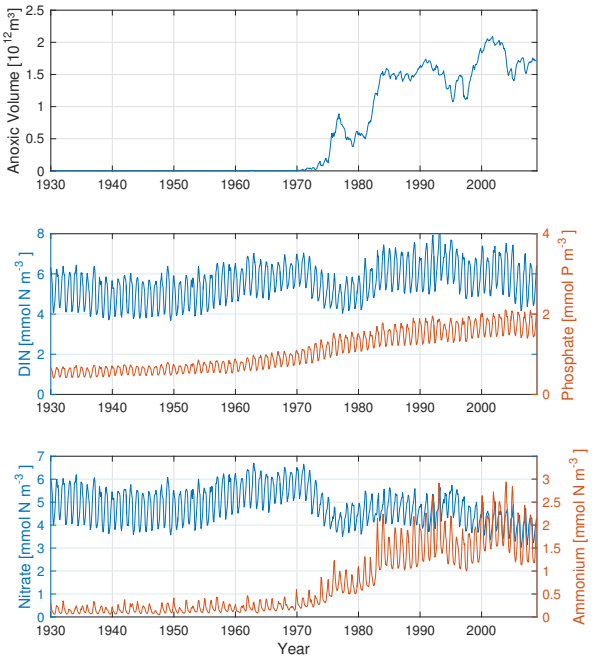

Figure 5. Time-series of anoxic volume (top), below mixed layer concentrations of DIN (nitrate + ammonium, blue) and phosphate (red) (middle) and nitrate (blue) and ammonium (red)(bottom).

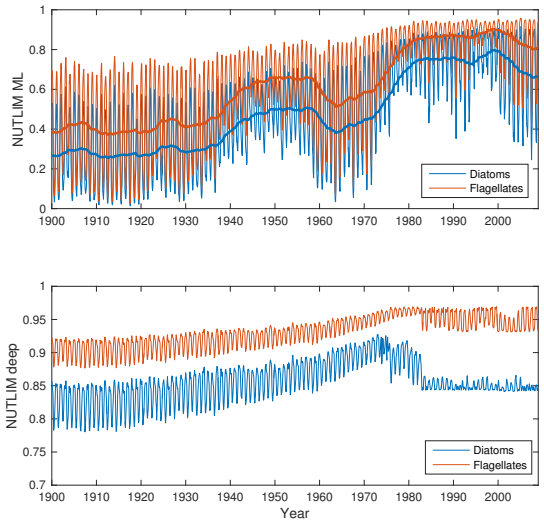

Figure 6. Time-series of nutrient limitation in the mixed layer (top) and below (bottom) for diatoms (blue) and flagellates (red). The thicker lines in the top panel show the 5yr moving average.

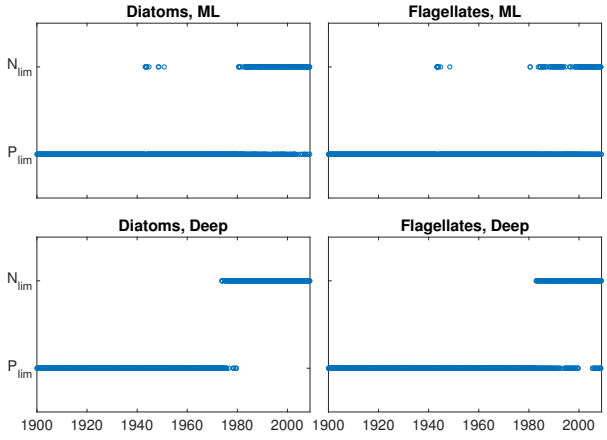

Figure 7. Nitrogen or phosphate limitation as function of time in the mixed layer (upper panels) and in the deep water (lower panels) of diatoms (left panels) and flagellates (right panels). Note that simultaneous N and P limitation is not possible although the size of the rings in the figures gives this appearence.

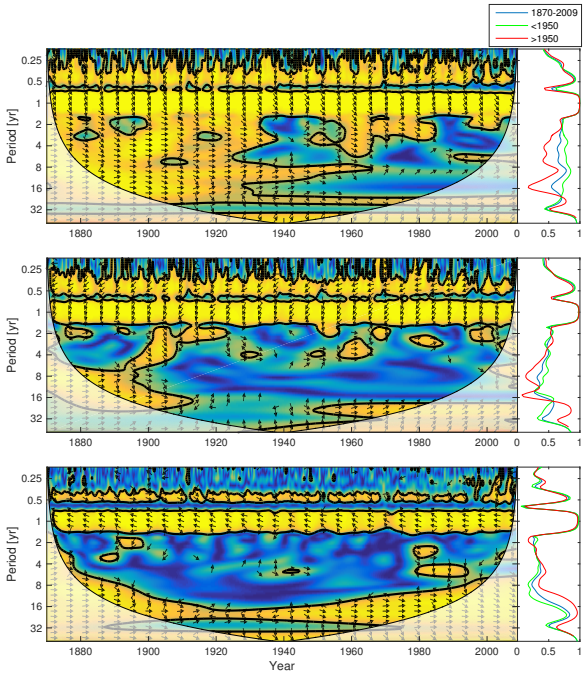

Figure 8. Wavelet coherence between mixed layer phosphate concentration and diatoms (top), flagellates (middle) and cyanobacteria (bottom). More yellow means more coherence. The arrows indicate the phase lag. When pointing to the right the two time-series are in phase and when pointing in the opposite direction anti-phase. The right panels show the coherence averaged over the whole period (blue) and before (green) and after (red) 1950.

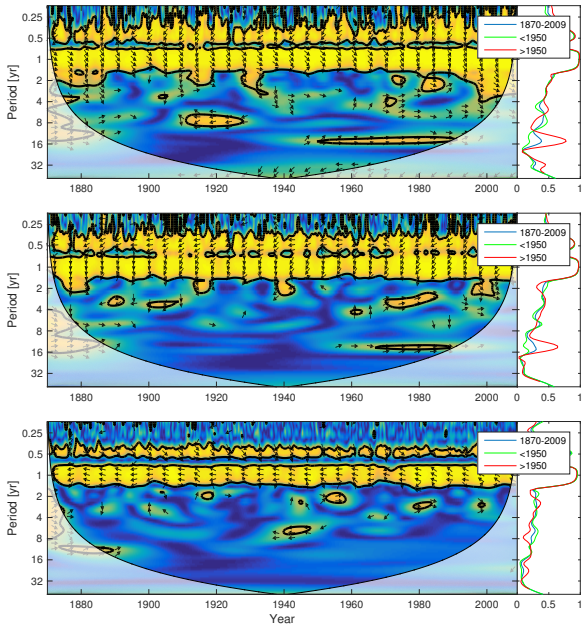

Figure 9. Wavelet coherence between mixed layer DIN concentration and diatoms (top), flagellates (middle) and cyanobacteria (bottom).

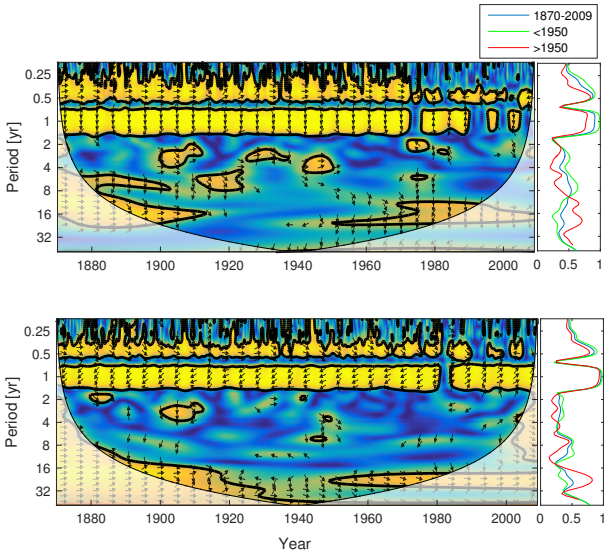

Figure 10. Wavelet coherence between deep water NUTLIM and diatoms (top), flagellates (middle)

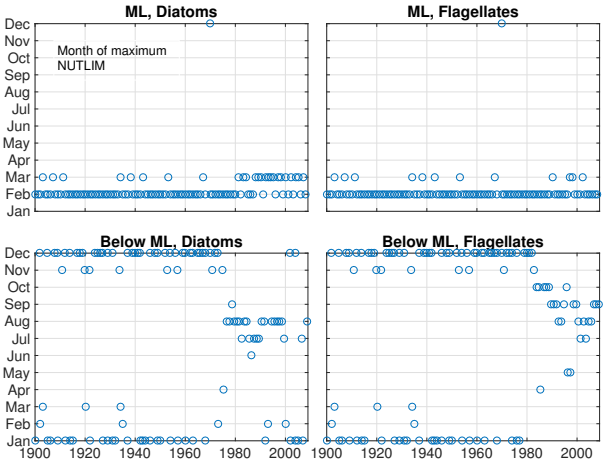

Figure 11. The month of maximum NUTLIM for diatoms (left) and flagellates (right) in the mixed layer (top) and below (bottom).

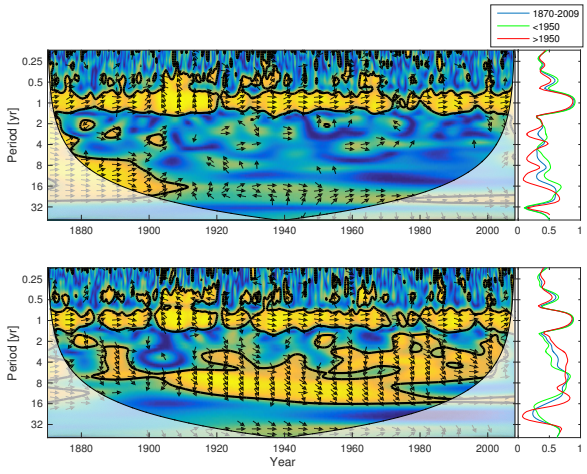

Figure 12. Wavelet coherence between riverine phosphate and mixed layer phosphate concentration (top) and riverine DIN and mixed layer DIN concentration (bottom). The arrows indicates the phase lag. When pointing to the right the two time-series are in phase and when pointing in the opposite direction anti-phase. The right panels show the averaged coherence for the whole period (blue) and before (green) and after (red) 1950.

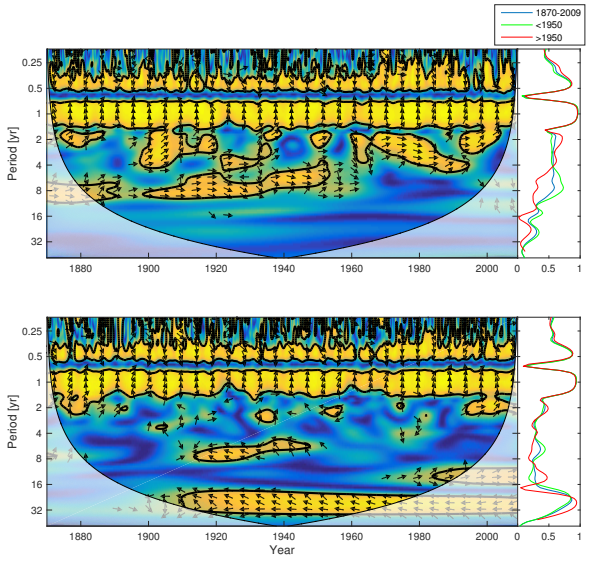

Figure 13. Wavelet coherence between mixed layer salinity and phosphate concentration (top) and mixed layer salinity and nitrate concentration (bottom). The right panels show the averaged coherence spectrum.

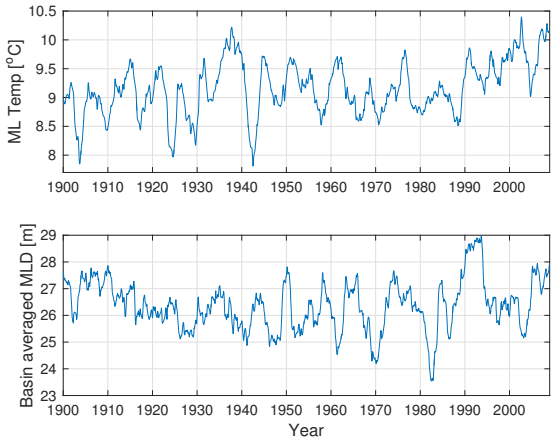

Figure 14. 2-yr moving average of mixed layer temperature (top) and mixed layer depth (bottom).

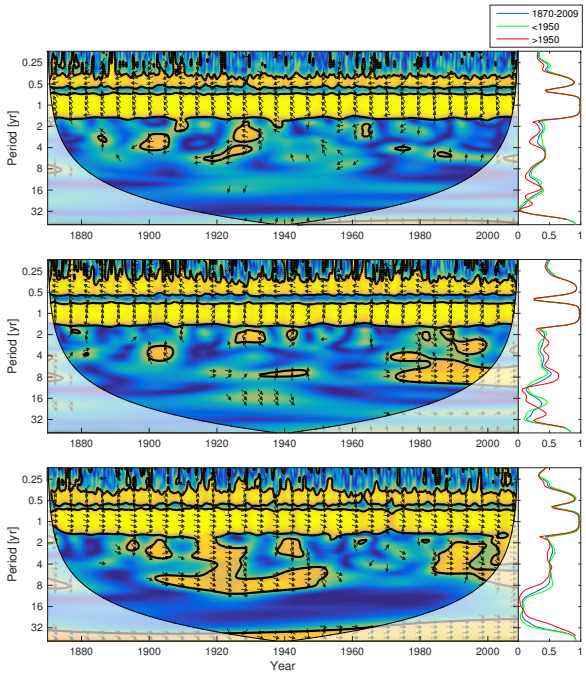

Figure 15. Wavelet coherence between mixed layer temperature and diatoms (top), flagellates (middle) and cyanobacteria (bottom).

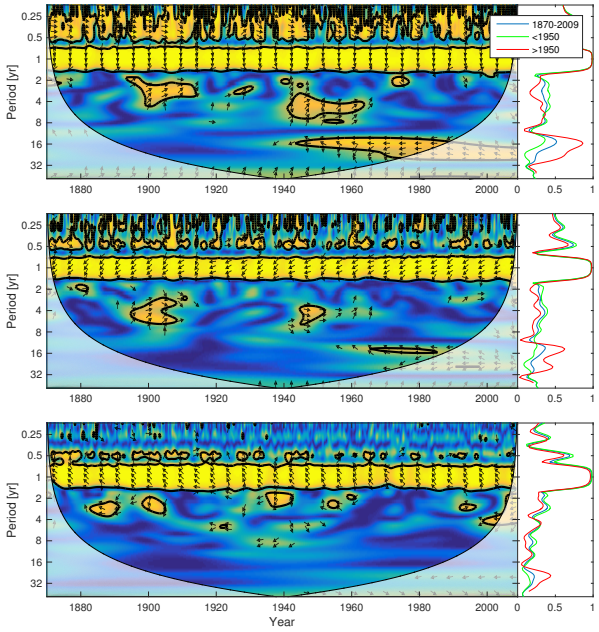

Figure 16. Wavelet coherence between mixed layer depth and diatoms (top), flagellates (middle) and cyanobacteria (bottom).